Experiments on upstream induction and wake flow for multirotor wind turbines

Experiments on upstream induction and wake flow for multirotor wind turbines

Jan Bartl[1], Idunn Koi[1], Morten Skoland[1], Gloria Stenfelt[1], Thomas Hansen[1]

[1] Dept. of Mech. and Marine Eng., Høgskulen på Vestlandet (HVL), Bergen, Norway

E-mail: jan.bartl@hvl.no

Abstract. Multirotor wind turbine concepts are increasingly discussed as cost-effective alternatives for floating wind energy installations. When multiple smaller rotors are installed next to each other, the individual rotors experience local blockage from their neighbours. Depending on the rotor arrangement, the flow through and around the multirotors will differ leading to a local variation in axial forcing and power output on the individual rotors. In this lab-scale experiment, we investigate how the spacing between the single rotors in a multirotor of seven actuator discs affects the upstream flow, thrust force distribution and downstream wake flow. Reducing the inter-rotor spacing is observed to cause larger zones of upstream velocity reductions, both in streamwise and lateral direction. Consequently, the difference in thrust force between a locally blocked central rotor and the surrounding rotors also increases for smaller rotor spacing. Measurements of the downstream wake flow behind a multirotor model indicate a lower initial velocity deficit compared to a single rotor. Reduced rotor spacing is found to increase the wake's initial velocity deficit and turbulence levels. Consequently, the wake recovers faster, resulting in similar velocity deficits independent of the rotor-spacing in the far wake region.

1. Introduction

While future offshore wind turbines increasingly will be installed on floating platforms, there is potential for a reduction in cost-of-energy when multiple smaller rotors are installed on one floating unit. Therefore, multirotor concepts have increasingly been discussed as an alternative for large offshore wind energy concepts during the last decade. A main advantage could be a relative reduction in material use for both floater and rotor blades per total rotor swept area as shown by Jamieson and Branney [1]. Further, favorable contributors to the cost-of-energy equation include a potential reduction in maintenance cost and an increase in operation time [2]. Despite these advantages, the design of a multirotor system also confronts us with numerous challenges, including the design of a low-drag support structure adapting to changing wind directions or a non-resonant aero-elastic design of the entire structure. Moreover, a number of basic questions regarding the aerodynamic performance of multirotor arrangements occur in the design process of multirotor systems. These include the optimal rotor layout, rotor number and inter-rotor spacing. When installed in a closely spaced arrangement, the rotors will experience local flow blockage, similar to very closely spaced wind farms [3] or fences of tidal stream turbines [4]. As a consequence, thrust forces and power production for centrally located rotors will be larger compared to their surrounding rotors. A computational study by Chasapogiannis et al. [5] on a multirotor setup of seven rotors (MR7), showed an overall thrust and power increase

of 1.5% and 3%, respectively. An extensive study by van der Laan et al. [6] on the Vestas multirotor demonstrator, consisting of 4 rotors (MR4), also showed a significant increase of overall power production. A simulation predicted power gains of 0–2%, which was confirmed by an increase in actual power measurements of 1.8% at below-rated wind speeds. These thrust and power gains are resulting from local flow blockage, which will furthermore influence both the upstream induction zone and the downstream wake flow of multirotor arrangements. Van der Laan et al. [6] also compared simulations and full-scale measurements of the wake flow behind the MR4 Vestas multirotor, indicating a faster wake recovery of a MR4-multirotor compared to an equivalent single rotor. Another study of the wake flow of a similar MR4 setup was performed with large-eddy simulations (LES) [7]. Results of this study also showed faster wake recovery, and indicated reduced turbulence levels in the near wake of a MR4 rotor. These trends were confirmed in an extensive LES-study of multirotor arrangements by Bastankhah and Abkar [8], investigating the effects of inter-rotor spacing, rotor number and rotational direction on the mean and turbulent wake characteristics. A larger rotor spacing was shown to result in lower velocity deficits in the near wake. Effects of increasing the number of rotors per total area is shown to be more complex: although velocity deficits are smaller in the near wake, a smaller recovery rate leads to slightly higher velocity deficits in the far wake. An experimental study on the wake interaction of two closely spaced wind turbines was presented by Maus et al. [9]. The study showed that both the inter-rotor distance and relative rotation of the two rotors have a significant effect on the flow entrainment into the combined wake of the two rotors. Power production and wake effects on a setup of a diffuser-augmented multirotor wind turbine were investigated experimentally by Göltenbott et al. [10]. They consistently observed higher power production on the central of the three turbines. The characteristics of the wake flow behind multirotors will be of particular interest when installing multirotors in farm arrangements. Multirotor wind farms have recently been investigated by van der Laan and Abkar [11]. Based on Reynolds-Averaged Navier-Stokes simulations they showed that a small MR4 farm could produce up to 1.7% more power than a farm of equivalent single rotors. Smaller separation distances were observed to be more favorable for multirotor (MR4) farms compared to single rotor farms. A similar trend was reported by Kirchner-Bossi and Porté-Agel [12], who showed that a tightly spaced multirotor farm could produce up to 6% more power than an equivalent single rotor farm. Additional layout optimisations on MR4 farms of different sizes consistently showed favorable results for multirotor farms.

In this paper, a lab-scale experiment on three simplified MR7 setups with different inter-rotor spacing is presented. The primary objective is to quantify how the inter-rotor spacing affects the upstream flow, thrust force distribution on the single rotor discs and downstream wake flow. Particular details on flow entrainment in the upstream induction zone and downstream wake flow will be discussed. The role of locally distributed turbulence generation is analysed and its effect on the wake recovery quantified. A secondary objective is to present a reference experiment for numerical wake flow simulations on simplified multirotor arrangements.

2. Methods

An experimental approach on three different setups of seven porous actuator discs, resembling a hexagonal arrangement of a MR7 wind turbine, is chosen. The simplified multirotor setups are moved through water in a towing tank, while the thrust force on each disc is measured with load cells. The upstream and downstream flow vector is measured by traversing an Acoustic Doppler Velocimeter at different lateral and streamwise upstream and downstream positions relative to the MR7 setup.

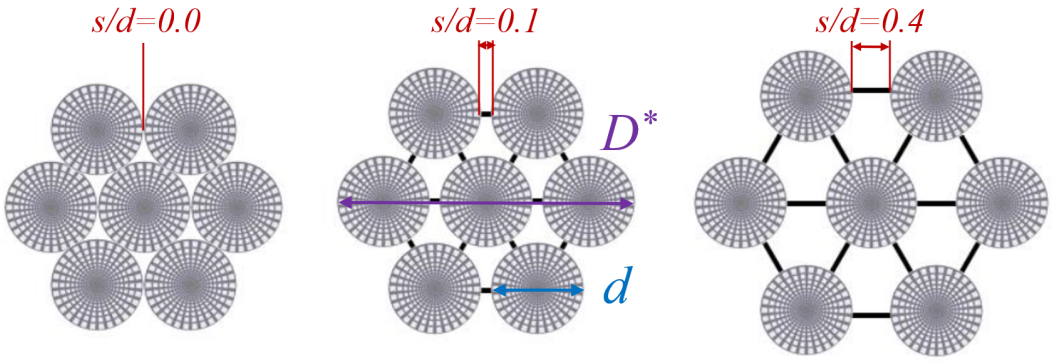

Figure 1. The three baseline setups of a multirotor, consisting of seven discs (MR7) with different inter-rotor spacings $s/d = 0.00$, 0.1 and 0.4, where d is a single disc's diameter, s is the inter-rotor spacing, D^* is the full edge-to-edge diameter of the MR7 setups.

2.1. Multirotor models

The porous discs are assembled into different multirotor arrangements. The laser-cut aluminum discs each have a diameter of $d = 200$ mm, thickness of $t = 5$ mm and a solidity of $\sigma = 57\%$. The thrust coefficient of the individual discs is measured to be $C_T = 0.94$, when no neighboring discs are present. The thrust coefficient is considered to be rather high compared to most wind turbines, but in the same range to some model wind turbines, e.g. the one used for a blind test wake experiment by Krogstad and Eriksen [13]. The discs are designed to resemble the effective solidity of rotating blades, i.e. with radially decreasing solidity towards the tip. The discs have trapezoidal holes, which are increasing in size with increasing diameter. The disc design is similar to previous wake experiments on discs performed in [14], [15] and [16]. Figure 1 shows the three setups of seven discs (MR7). A single disc diameter is denoted with d and the inter-rotor spacing with s. When discussing downstream distances in section 3, two more reference diameters $D = 3d$ and the total edge-to-edge diameter $D^* = 3d+2s$ will be introduced. In this experiment, inter-rotor spacings of $s/d = [0.0, 0.1, 0.4]$ are investigated. Each disc centre is connected via a hexagonal support structure. The cylindrical rods of this structure have a diameter of 10 mm. The centre of the multirotor structure is connected to a tower, which has a diameter $d_{\text{tower}} = 20$ mm and a submerged depth $h_{\text{tower}} = 1000$ mm, as illustrated in Figure 2. At this depth, the multirotor model is observed to have a negligible influence on wave shedding on the water surface.

2.2. Towing tank

The wake characteristics are investigated by towing the multirotor setups in the MarinLab towing tank at the Western Norway University of Applied Sciences (HVL). The towing tank is 50 m long, 3 m wide and 2.2 m deep. Towing tank experiments on wind turbine wakes have previously been performed by Barber et al. [17] and Kress et al. [18]. This is possible due to the fact that both water and air behave as Newtonian fluids at low speeds. The kinematic viscosity of the fresh water is $\nu = 1.1386 \cdot 10^{-6}$ m^2/s at 15°C. Figure 2 shows a sketch of the measurement setup in the towing tank. The multirotor model is mounted on a first towing carriage, while the ADV is fixed to an automated traverse on a second carriage. The carriages are connected via a steel wire and distance in x-direction between them can be varied. The automated traverse allows for a lateral movement of the ADV probe in y-direction.

2.3. Measurement techniques

In this set of experiments a towing velocity of $u_0 = 0.50$ m/s is chosen. The three-dimensional velocity vector is measured by a Nortek *Vectrino+* Acoustic Doppler Velocimeter (ADV) a sampling frequency of $f_{\text{sample}} = 200$ Hz. Further details on the measurement device and seeding particles are documented in [19]. The thrust forces on the single discs are measured individually on the central and two edge discs of the MR7 setup. Small custom load cells based on a Wheatstone bridge of strain gauges measure the axial forces directly between the individual discs and the support structure. In this way, drag from the support structure and tower are bypassed. The Reynolds number in this experiment is $Re_d \approx 10^5$, which is based on a single disc diameter d. This is about two orders of magnitudes smaller than for full-scale multirotor concepts, but in a similar range as most lab-scale experiments in a post-critical Reynolds regime.

2.4. Measurement locations

Upstream and downstream flow measurements are carried out to be able to compare both the induction zone as well as the wake flow of the three configurations. The measurement locations are shown in Figure 3. Upstream measurements are performed at x/d = -3.0, -2.0, -1.4, -1.0 and -0.4. The same distances were chosen for measurements of the very near wake, i.e. $x/d = 0.4$,

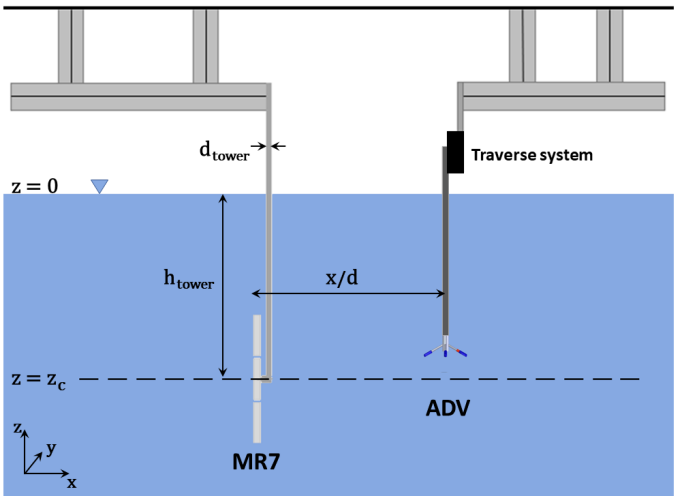

Figure 2. Sketch of two carriages above the water tank. The carriages are connected through a wire. The first carriage is connected to the MR7 model, the second one to the ADV traverse.

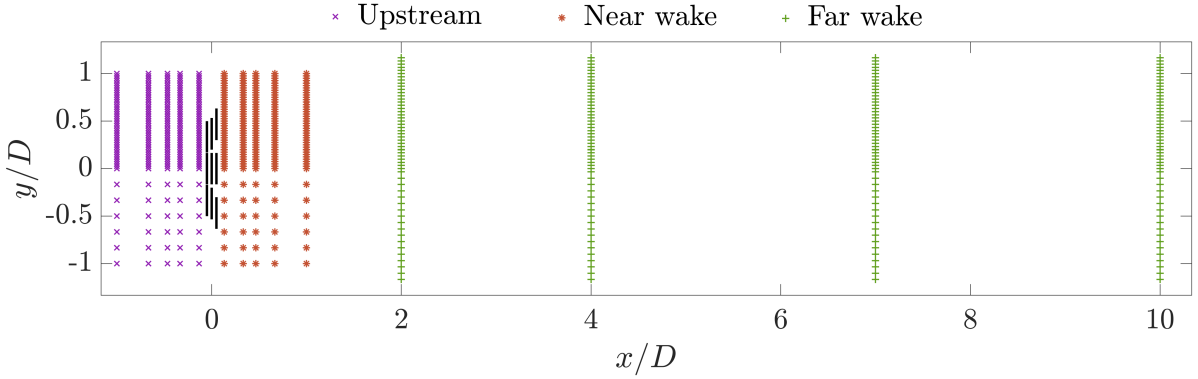

Figure 3. Measurement locations of the point measurements upstream, and in the near and far wake downstream of the three multirotor setups.

1.0, 1.4, 2.0 and 3.0. Measurements in the wake further downstream were performed at x/D = 2, 4, 7 and 10. For both upstream and wake measurements, the symmetrical setup allows for measurements of only half a wake profile. For all measurement distances, control measurements in the other half of the wake are performed to ensure that the symmetry assumption is correct. Since there are stronger gradients upstream and in the near wake of the turbine, the spacial resolution is chosen to be higher than for the far wake. All wake measurements are performed at the water depth of the turbine centre, z_c = -1000 mm as shown in Figure 2.

3. Results

The results are presented in three sub-sections, describing the upstream flow in the induction zone, the thrust force distributions on the individual rotors and the downstream flow in the wake.

3.1. Upstream flow

The upstream induction zones of the three MR7 setups are compared by the means of velocity contours in Figure 4. It is observed that the central discs experience larger upstream velocity reductions than the edge discs. The high velocity reduction can be attributed to the higher local blockage ratios on the central discs. For a very tightly spaced MR7 setup with s/d = 0.0, the velocity reduction in front of the central disc is higher than for larger spacings. The contour plots also demonstrate how the individual induction zones of the discs merge into one global induction zone further upstream. Small velocity reductions are observed at three single rotor diameters upstream for all MR7 configurations. The most tightly spaced setup clearly has the largest upstream induction effect of the three tested configurations.

A similar induction zone upstream of a row of aligned wind turbine rotors has previously been presented in a computational study by Meyer Forsting et al. [20]. The major difference between their setup and the present setup is that, here there is one more row of two rotors both above and below, leading to even higher local blockage and thus a larger upstream velocity decrease.

Figure 5 is based on the same data that is presented in the contour, but instead velocity profiles at the actual measurement locations are compared at different upstream locations. Since

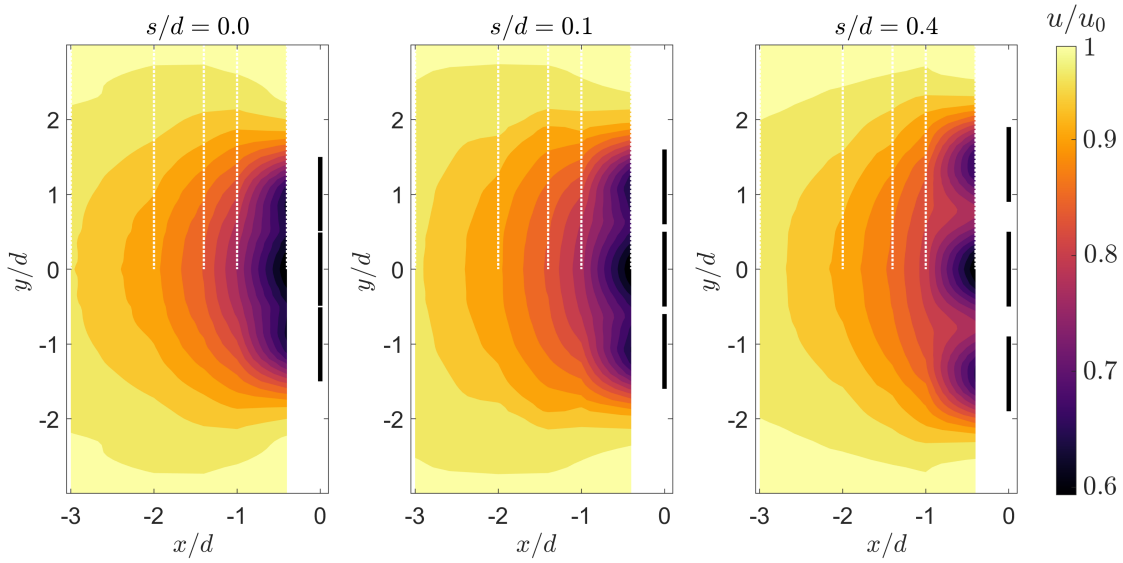

Figure 4. Contours of streamwise velocity in the upstream induction zone of three MR7 setups: a) s/d = 0.0 b) s/d = 0.1 c) s/d = 0.4.

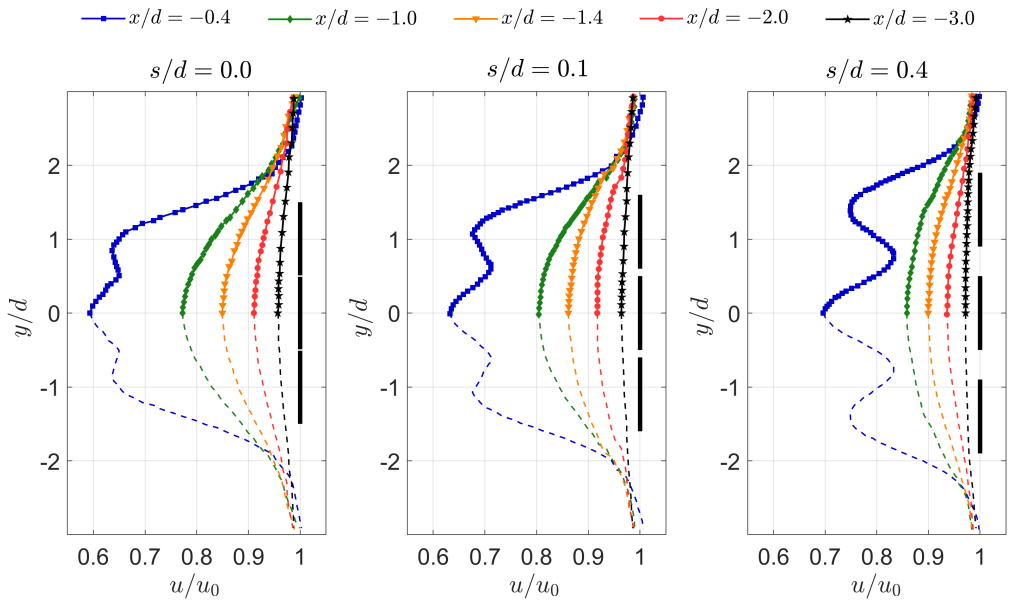

Figure 5. Streamwise velocities profiles in the upstream induction zone of three MR7 setups: a) $s/d = 0.0$ b) $s/d = 0.1$ c) $s/d = 0.4$.

only half the velocity profile is measured in high resolution, the results are mirrored around the centre. At the closest upstream location x/d = -0.4, the setup with spacing $s/d = 0.0$ shows a velocity reduction of 41% in front of the central disc, compared to 37% for $s/d = 0.1$ and 31% for $s/d = 0.4$. When comparing the upstream induction of the different setups, also the lateral expansion of the upstream flow is relevant. Figure 6 therefore compares velocity profiles

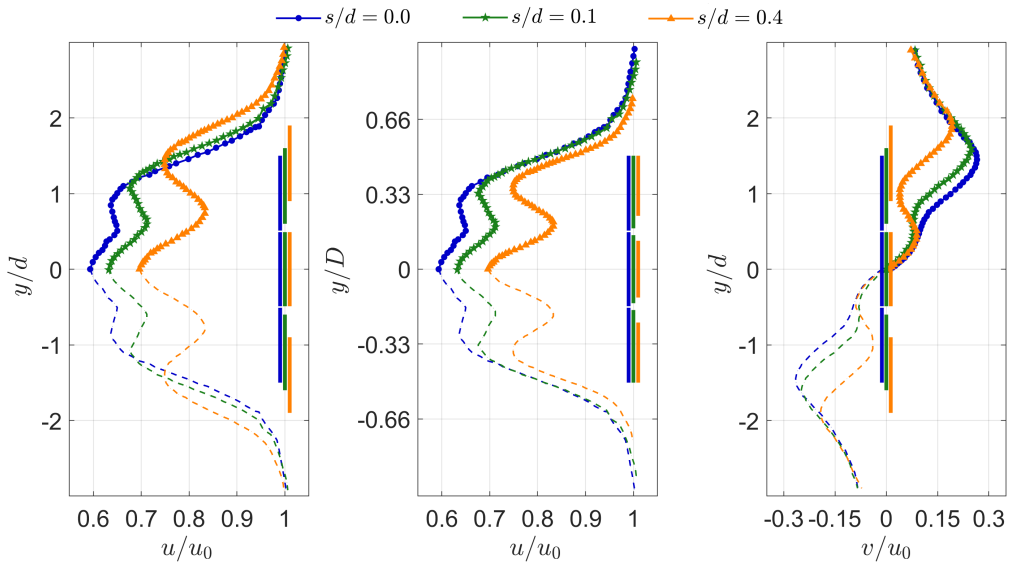

Figure 6. Comparison of velocity components measured in the upstream induction zone of three MR7 setups at x/d = -0.4: a) Absolute expansion with single disc diameter d as a reference b) Relative expansion referred to total multirotor diameter D = [600 mm, 640 mm, 780 mm] c) Crossflow velocities measured in y-direction, normalised with single rotor diameter d.

measured at x/d = -0.4 directly for all three MR7 configurations. The leftmost figure shows the induction zones' absolute expansion, with a single disc diameter d as a reference. Unsurprisingly, the induction zone of the largest MR7 setup with $s/d = 0.4$ expands the most. If referred to the total MR7-diameter D of each configuration, however, the same setup has the smallest relative induction zone expansion (central figure). As the global blockage is smaller in this case, i.e. more flow is admitted through the gaps in the centre of the MR7, and less flow has to bypass the setup. This reasoning is confirmed by an analysis of the cross-flow velocities v/u_0 as shown in the right of Figure 6. The tightly spaced rotor setups deflect a major part of the flow to the left and right, while the additional second peak in v/u_0 in the orange line indicates flow deflections towards the gaps surrounding the central disc in the case of a larger spacing of $s/d = 0.4$.

3.2. Force distribution

In Figure 7 the individual thrust coefficients measured on the central and two edge discs are compared. For the two edge discs, the average of the forces is shown. Error bars represent the standard deviations of repeated measurements. The black dots represent the thrust coefficient measured for an isolated, unblocked disc, i.e. when no neighboring discs are present. It can be observed that thrust forces on the blocked central disc are higher than for an isolated disc. For the closest spacing of $s/d = 0.0$, an increase in thrust of 10% on the central disc is measured compared to the thrust measured on an isolated disc. When increasing the inter-rotor-spacing, and thus reducing the local blockage, this difference becomes significantly smaller. The results furthermore show that thrust forces on the edge discs are approximately in the same range as the thrust on an isolated disc. As shown in the above sub-chapter on upstream flow, the edge discs might experience slightly asymmetric inflow due to being blocked on only one side. Despite these effects, the resulting thrust seems to be similar to the isolated case. When comparing the total thrust of the MR7 setups to seven times the thrust on an individual disc, the total thrust on the multirotor is slightly higher for all cases. For an inter-turbine spacing of $s/d = 0.1$, an increase of 2.9% in total thrust for the multirotor is measured. This result shows the same trend as the thrust increase of 1.5% found in the numerical simulation by Chasapogiannis et al. [5], in which they used a MR7 setup with a rotor spacing of $s/d = 0.05$. The baseline thrust coefficient of a single rotor was not specified in their paper.

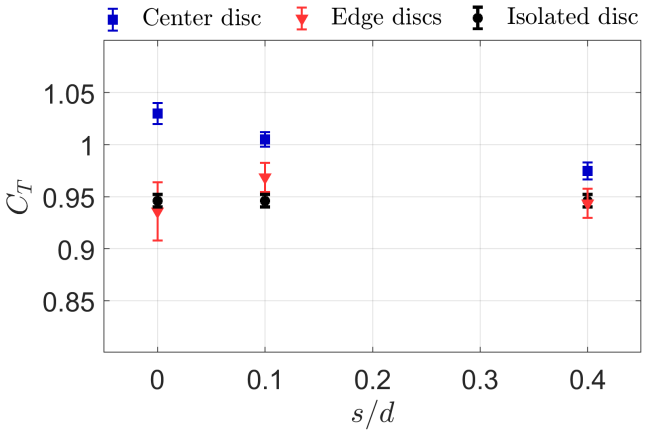

Figure 7. Comparison of the individual thrust coefficients C_T on the central disc vs. edge discs for different inter-rotor spacings s/d. The thrust coefficient of an unblocked single disc is shown with black dots for reference.

3.3. Downstream wake flow

The mean velocity contours in the wakes of the three MR7 configurations with different inter-rotor spacing are compared in Figure 8. Similar to previous investigations of multirotor wakes, a reference diameter of $D = 3d$ defines the downstream distances x/D. It is observed that the individual rotor wakes start merging into a larger, Gaussian-shaped wake at a downstream distance between $x/D = 2$ and 4. For increased inter-rotor spacing the individual rotor wakes are seen to travel a longer distance before they start interacting with their neighbouring wakes. Thus, the transition process into a larger wake is shifted further downstream for increased rotor-spacing. This observation confirms simulation results on the effect of inter-rotor spacing presented on a MR4 wake by Bastankhah and Abkar [8].

For a more detailed comparison of the velocity recovery in the wake, cross-sectional profiles of the mean velocity at four downstream distances are compared in Figure 9. In addition to the mean velocity, profiles of the normalised turbulent kinetic energy tke/u_0^2 are presented in the row below. At $x/D = 2$ the wake behind all three setups has already transitioned into one large Gaussian-shaped wake. The velocity deficit is notably the smallest for the largest inter-rotor spacing. Comparing the profiles of turbulent kinetic energy at the same downstream distance, an interesting observation is made. A top-hat shaped, rather flat turbulence profile is

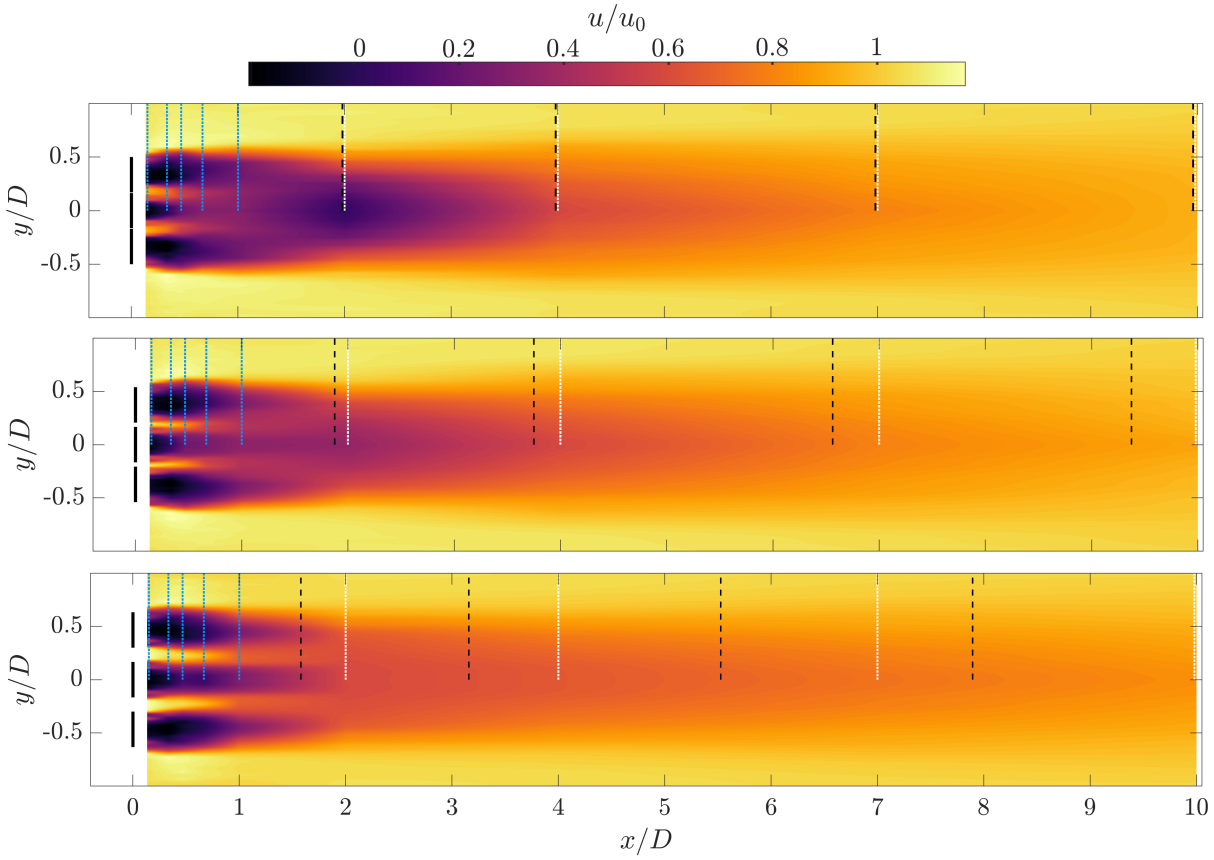

Figure 8. Contours of normalised mean velocity u/u_0 behind multirotor 7 (MR7) setups with inter-rotor spacings of $s/d = 0.0$, 0.1 and 0.4. Blue and white dotted lines show actual measurement locations, while coloured values are linearly interpolated. Black dashed lines indicate where wake cross sections at x/D=[2, 4, 7, 10] could be compared, if the full edge-to-edge diameter D^* would be used as a reference, i.e. x/D^*=[2, 4, 7, 10], for all configurations.

measured behind the largest rotor spacing. At the same location, the two tightly-spaced rotor configurations produce two distinct turbulence peaks around the multirotors' edges, in a similar manner as for large single rotor wakes. This could possibly be explained by a higher turbulence production in the multirotor centre, specifically around the edges of the central disc, for the largest inter-rotor spacing. Flow of high kinetic energy in between the individual rotors could have stimulated the mixing in the centre of the wake and simultaneously helped to break down larger turbulent structures around the main edges. Further downstream, at $x/D = 4$, the wakes behind the two most tightly spaced multirotors have significantly reduced, showing a very similar velocity deficit. It is noteworthy to mention, that the peak velocity in the wake MR7 with zero inter-rotor spacing has recovered by about 50% from $x/D = 2$ to 4, while the recovery rate for the setups with larger spacing is observed to be smaller. Rotor-generated shear stresses in the wake flow are assumed to be the main driver for wake recovery. At $x/D = 7$, the velocity profiles behind the three configurations practically lie on top of each other. Again, higher wake recovery rates driven by higher turbulence levels in the wakes of the tighter spaced rotors are suspected to be the main cause for this development. At the same location, the profiles of turbulent kinetic energy for $s/d = 0.0$ and 0.1 have equalised, while still being about double as high as the profile for $s/d = 0.4$. At the furthest downstream measurement at $x/D = 10$, the velocities behind the two most tightly spaced rotors notably were slightly lower than for the large spacing. The increased wake recovery rates of the two tighter spaced multirotors have ultimately resulted in a slightly weaker wake at this far downstream location. This trend confirms observations made

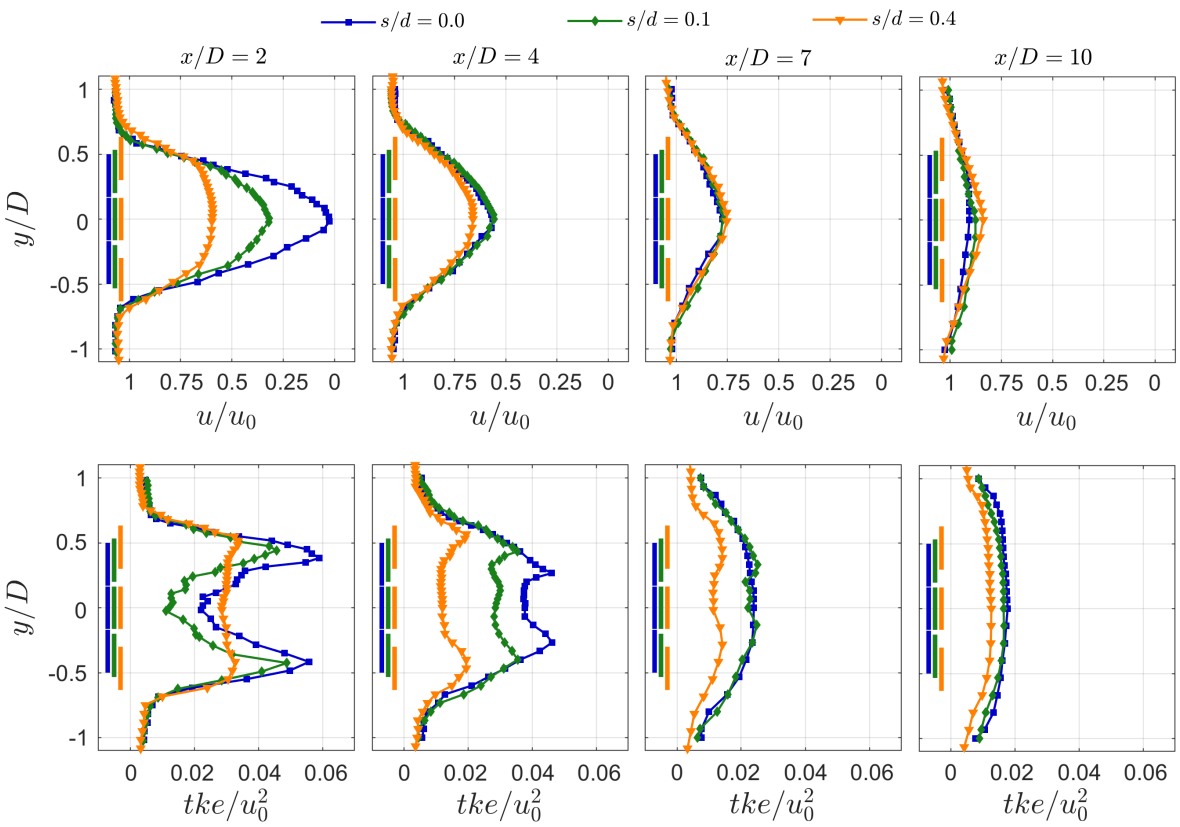

Figure 9. Normalised mean velocity u_{mean}/u_0 (first row) and turbulent kinetic energy tke/u_0^2 (second row) for inter-rotor spacings $s/d = 0.0$, 0.1 and 0.4 behind a MR7 compared at four downstream distances x/D=2, 4, 7 and 10.

by Bastankhah and Abkar [8] in an MR4 wake, where the wake recovery behind more tightly-spaced rotor setups was detected to overtake the recovery behind largely-spaced setups in the far wake. These results indicate that multirotor systems with larger inter-rotor spacing could potentially be set up closer to each other when arranged in wind farms. However, the influence of several atmospheric parameters, in particular atmospheric turbulence, needs to investigated in future studies. Another important discussion involves the reference diameter D or D^*, which is chosen to compare multirotor wakes at a specific downstream distances x/D or x/D^*. This choice of reference diameter might influence the presented findings on how the wake looks at the normalised downstream distances. The change of downstream reference locations is indicated by the black dashed lines in Figure 8, where locations at $x/D = 2$, 4, 7, 10 are significantly moved closer towards the turbines when regarded as $x/D^* = 2$, 4, 7, 10. Therefore, a more thorough discussion on multirotor wakes with different reference diameters is needed.

4. Conclusions

This study indicates that local blockage effects increase the local thrust forces on centrally located rotors in multirotor wind turbines. A tighter rotor spacing leads to higher thrust and increase in the local induction in the upstream flow field. The lateral expansion of the upstream flow field is observed to decrease with increasing distance between the actuator discs, relative to the total diameter of the multirotor. Comparing the wake flow, larger inter-rotor spacing leads to a lower mean velocity deficit in the wake at $x/D = 2$ and 4. At these locations, the rotor-generated turbulence is observed to have a flat top-hat shape for the largest inter-rotor spacing, while distinct turbulence peaks around the edges dominate. In the far wake at $x/D = 7$ and 10, however, the velocity deficits behind the three multirotor configurations are observed to be rather similar. These results suggest that larger inter-rotor spacing in multirotors might make it possible to decrease the spacing between the multirotor units in a wind farm setup. Future work will also investigate the influence of ambient turbulence and rotor number on the recovery of multirotor wakes. Moreover, a framework of computational flow simulations coupled to numerical optimisation is currently being established to further investigate what inter-rotor spacing should be chosen for optimal multirotor performance in wind farm setups.

References

[1] Jamieson P and Branney M 2012 *Energy Proced* **24** 52–59
[2] McMorland J, Pirrie P, Collu M, McMillan D, Carroll J, Coraddu A and Jamieson P 2022 *J Phys Conf Ser* **2265** 042059
[3] McTavish S, Rodrigue S, Feszty D and F N 2015 *Wind Energ* 1989–2011
[4] Nishino T and Willden R 2012 *J Fluid Mech* **708** 596–606
[5] Chasapogiannis P, Prospathopoulos J, Voutsinas S and Chaviaropoulos T 2014 *J Phys Conf Ser* **524** 012084
[6] vdLaan P, Andersen S, García N, Angelou N, Pirrung G, Ott S, Sjöholm M, Sørensen K, Neto J, Kelly M, Mikkelsen T and Larsen G 2019 *Wind Energ Sci* **4** 251–271
[7] Ghaisas N, Ghate A and Lele S 2018 *J Phys Conf Ser* **1037** 07202
[8] Bastankhah M and Abkar M 2019 *Phys Fluids* **31(8)** 085106
[9] Maus J, Peinke J and Hölling M 2022 *J Phys Conf Ser* **2265** 042064
[10] Göltenbott U, Ohya Y, Yoshida S and Jamieson P 2017 *Renew Energ* **112** 25–34
[11] vdLaan P and Abkar M 2019 *J Phys Conf Ser* **1256** 012011
[12] Kirchner-Bossi N and Porté-Agel F 2020 *J Phys Conf Ser* **1618** 032014
[13] Krogstad P A and Eriksen P 2013 *Renew Energ* **50** 325–333
[14] Bossuyt J, Howland M, Meneveau C and Meyers J 2017 *Exp Fluid* **58**
[15] Helvig S d J, Vinnes M K, Segalini A, Worth N A and Hearst R J 2021 *J Wind Eng Ind Aerod* **209** 104485
[16] Neunaber I, Hölling M, Whale J and Peinke J 2021 *Renew Energ* **179** 1650–1662
[17] Barber S, Wang Y, Jafari S, Chokani N and Abhari R 2011 *J Sol Energy Eng* **133** 011007
[18] Kress C, Chokani N and Abhari R 2016 *Renew Energ* **89** 543–551
[19] Bartl J, Aasnæs C, Bjørnsen J, Stenfelt G and Lande-Sudall D 2022 *J Phys Conf Ser* **2362** 012004
[20] Meyer Forsting A R, Troldborg N and Gaunaa M 2017 *Wind Energ* **20** 63–77